Desalination and Water Treatment
www.deswater.com

doi: 10.5004/dwt.2018.21977

109 (2018) 241–252
March

Efficient removal of malachite green dye from aqueous solution using functionalized GO/Fe_3O_4 nanocomposite: kinetic, equilibrium and thermodynamic studies

Sheng Feng[a,*], Shuguang Liu[a], Zhihui Zhang[b], Shanshan Feng[a], Bin Yuan[a], Ping Cheng[a], Runbai Wang[a]

[a]*School of Environmental and Safety Engineering, Changzhou University, Jiangsu 213164, China, Tel. +86 519 86330080; emails: shfeng@cczu.edu.cn (S. Feng), shguangliu@163.com (S. Liu), fss728@163.com (S. Feng), yuanbinbn@163.com (B. Yuan), 15189703919@163.com (P. Cheng), ruibaiwang@163.com (R. Wang)*
[b]*Jiangsu Key Laboratory of Advanced Catalytic Materials and Technology, Changzhou University, Jiangsu 213164, China, email: zhangzh@cczu.edu.cn*

Received 9 August 2017; Accepted 1 February 2018

ABSTRACT

In this work, we have revealed efficient solvothermal method for the synthesis of the graphene oxide (GO)/magnetite (Fe_3O_4) nanocomposite for the removal of malachite green (MG) from aqueous solution. The nanocomposite was characterized by X-ray diffraction, scanning electron microscopy, transmission electron microscopy, nitrogen adsorption–desorption and vibrating sample magnetometer isotherm analysis. Using adsorption models for equilibrium and kinetic investigation, it was found that the goodness of mathematical fitting of the batch adsorption data on the adsorption isotherms conformed well to the Langmuir isotherm, and the kinetic models could be described by the pseudo-second-order model. The thermodynamic parameters reveal that the adsorption process is spontaneous and endothermic in nature. The prepared GO/Fe_3O_4 nanocomposite showed excellent efficient removal of MG (over 98% for 1.0 g L^{-1}) with high adsorption capacity (220 mg g^{-1}) and rapid separation from water by an external magnetic field because of the efficient combination of the advantages of GO and the Fe_3O_4 nanoparticle. These results proved that the preparation of GO/Fe_3O_4 nanocomposite can be used as an efficient, separable adsorbent to adsorb MG contaminants in water.

Keywords: Graphene oxide; Fe_3O_4; Malachite green; Adsorption; Magnetite; Recycle

1. Introduction

Various kinds of synthetic dyes have been used as important raw materials for colorants in a variety of industries such as textiles, leather, paper, wool, cosmetics and printing. However, if released into water, synthetic dyes may pose a significant threat to the environment and human beings due to their toxic and even carcinogenic effects [1–4]. As a basic dye, malachite green (MG) is a cationic triphenylmethane dye which has been widely used as a strong antifungal, antibacterial and antiparasitical agent [5–7]. But many studies indicate that MG is environmentally persistent and acutely toxic to aquatic and terrestrial animals, which may result in teratogenic, carcinogenic and mutagenic effects on the human body [8–10]. Therefore, it is highly necessary to develop effective methods to remove MG from the environment. Commonly, MG wastewater treatment methods include adsorption, flocculation, electrolysis, membrane filtration, biooxidation and so on [11–14]. Of these, the adsorption technology is regarded as one of the most effective methods to remove dye pollutants. Typical adsorbents are molecular sieve, adsorption resin, activated carbon and its

* Corresponding author.

derivatives [15]. They are low in adsorption efficiency and are difficult to separate and recover. As a consequence, there is pressure to develop new adsorbents with low cost, high adsorption capacity and good recyclability.

Graphene is a new type of single-atom two-dimensional material which has a wide application prospect in optical, electrical and thermal fields [16,17]. Graphene oxide (GO) as its important derivative, contains a large number of hydroxyl, carboxyl and a variety of oxygen-containing functional groups, can fix metal or metal oxide to its surface [18]. Meanwhile, magnetite (Fe_3O_4 NPs) has the advantage of small size and large surface area [4]. In the immobilized enzyme carrier biochemical products such as separation, catalysis and other fields are widely used [19]. The GO/Fe_3O_4 nanocomposite, which is prepared by combining iron oxide and GO, can take advantages from both. The separation and recovery will proceed quickly and efficiently under external magnetic field to avoid secondary pollution [20].

In this context, a novel GO/Fe_3O_4 nanocomposite for efficient MG adsorption from aqueous solution was synthesized using a simple solvothermal method as shown in Fig. 1. The kinetics and thermodynamics of the dye adsorption on the GO/Fe_3O_4 nanocomposite have been investigated. The resulting GO/Fe_3O_4 nanocomposite could be utilized as a magnetically separable and efficient adsorbent for dye removal from water.

2. Experimental methods

2.1. Materials

All reagents were purchased from Sinopharm Chemical Reagent Co., Ltd, China, and used without further purification. They included iron chloride hexahydrate ($FeCl_3{\cdot}6H_2O$), sodium acetate (NaOAc), sodium hydroxide (NaOH), hydrochloric acid (HCl), graphite powder, anhydrous ethanol, potassium permanganate and sulfuric acid, hydrogen peroxide (30%) and MG. Deionized water was used in the synthesis and all treatment processes.

2.2. Preparation of graphene oxide

GO was prepared from expandable graphite powder according to the modified Hummers method [21]. First, 23 mL of concentrated sulfuric acid was added into a 250 mL flask and cooled by immersing it into ice bath, then 1.0 g of graphite powder and 1.0 g of $NaNO_3$ were gradually added into the flask and electromagnetically stirred for 1 h. Subsequently, 10 g of $KMnO_4$ was slowly added under stirring at temperature below 283 K, the stirring process maintained for about 2 h. Next, the ice bath was removed out and the mixture cooled and kept at room temperature overnight. 40 mL cooled water was slowly added into the flask with continuous stirring and the temperature maintained at 363 K in the water bath for 0.5 h. In the next step, 140 mL water and 10 mL of 30% (v/v) H_2O_2 were added to quench the reaction. Then, the centrifugation and repeated rinsing with 10% HCl were performed until there is no precipitation phenomenon. Finally, the generated brown powder of graphite oxide was dried at 353 K under vacuum for 12 h for further reactions.

2.3. Preparation of GO/Fe_3O_4 nanocomposite

Preparation of GO/Fe_3O_4 nanomaterials was carried out using the solvothermal method. The as-prepared GO (0.5 g) was exfoliated by ultrasonication in 80 mL of ethylene glycol for more than 3 h. 1.6 g $FeCl_3{\cdot}6H_2O$ and 3.2 g NaOAc were then dissolved in a GO ethylene glycol solution at ambient temperature. After stirring for about 30 min, the solution was transferred into a 100 mL Teflon-lined stainless steel autoclave and kept at 473 K for 6 h followed by cooling to room temperature naturally. The black precipitate was centrifuged, washed several times with ethanol, and finally dried at 333 K for 12 h in a vacuum oven to yield GO/Fe_3O_4 nanocomposite.

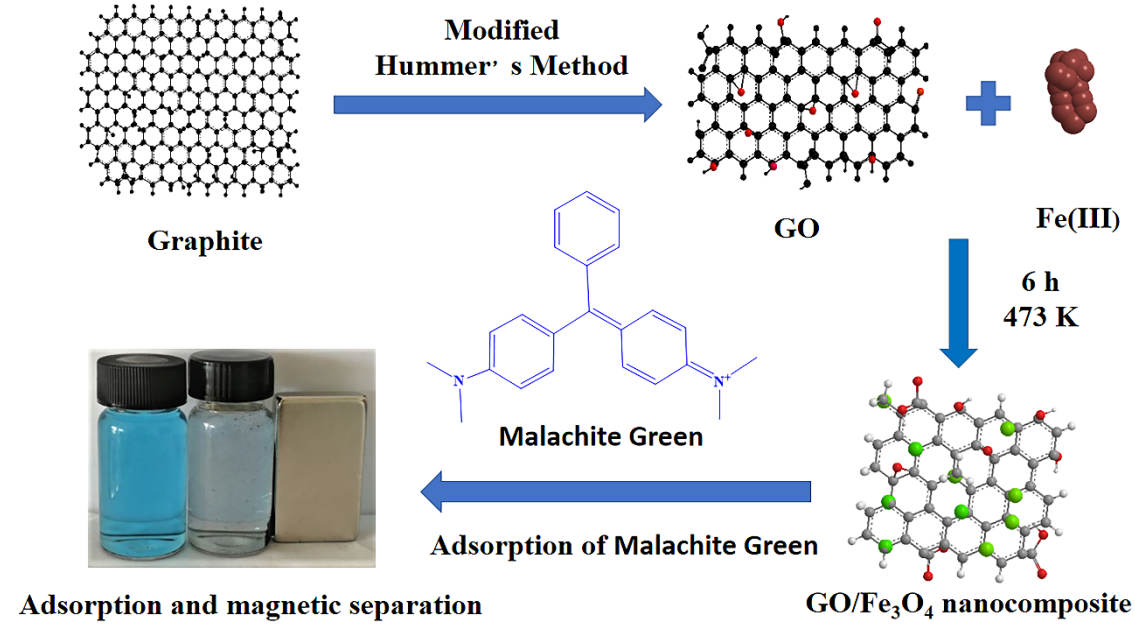

Fig. 1. Schematic illustration of the synthesis of the GO/Fe_3O_4 nanocomposite serving as magnetic adsorbent for MG uptake.

2.4. Characterization

The powder X-ray diffraction (XRD) measurements were recorded on a Dmax/Ultima IV diffractometer (Rigaku, Japan) with monochromatized Cu Kα_1 radiation (λ = 0.15418 nm). Morphological changes were analyzed using a ZEISS Supra 55 microscope (SEM). Diameter distribution was determined by measuring at least 100 random nanoparticles in the SEM images. The diameters of nanoparticles were analyzed using software Image J 1.3s. The microstructure of the sample was observed by transmission electron microscopy (TEM) (JEM-2100, JEOL, Japan) N_2 adsorption isotherms were obtained using ASAP 2020 instrument (Micromeritics, USA). The samples were outgassed at 393 K for 8 h before measurements. The specific surface area was calculated by the Brunauer–Emmett–Teller (BET) method. Magnetization measurements were carried out using a vibrating sample magnetometer (VSM, 7404, Lake Shore, an applied magnetic field of 300 Oe at room temperature) under applied magnetic field at room temperature.

2.5. General procedures for the adsorption experiments

The adsorption of MG in aqueous solution on the as-prepared GO/Fe_3O_4 nanocomposite was performed in a batch experiment. First, 0.01 g of GO/Fe_3O_4 nanocomposite was added to 50 mL of the initial concentration of MG solution; the use of constant temperature oscillator at 200 r min^{-1} speed of oscillation for 10 h. The adsorption temperature was 333 K, and the pH of the solution was adjusted with dilute hydrochloric acid or sodium hydroxide to 3–9, respectively. The concentration of the adsorbed dye was measured after magnetic separation. The adsorption calculation formula:

$$q_e = \frac{(c_0 - c_e)}{m} \times V \quad (1)$$

where q_e (mg·g^{-1}) is the amount adsorbed per gram of adsorbent; c_0 and c_e are the initial and equilibrium concentrations of MG in the solution (mg L^{-1}), respectively; m is the mass of the adsorbent used (g) and V (L) is the initial volume of the MG solution.

2.6. Desorption experiments

For the desorption study, 0.01 g GO/Fe_3O_4 nanocomposite was added to 50 mL of MG solution (60 mg L^{-1}) and shaken in a 200 r min^{-1} water bath shaker for 10 h. After magnetic separation, the supernatant was withdrawn to analyze the remaining MG concentration. The adsorbent was treated by ultrasound for 1 h after adding 25 mL of ethanol (pH 3.0) to achieve complete desorption. The adsorption–desorption process of MG was repeated four times.

3. Results and discussion

3.1. Characterization of GO/Fe_3O_4 nanocomposite

In this work, the GO/Fe_3O_4 nanocomposite was prepared according to the reported procedure [22].

In order to investigate the morphology of the products, scanning electron microscopy (SEM) analysis and TEM

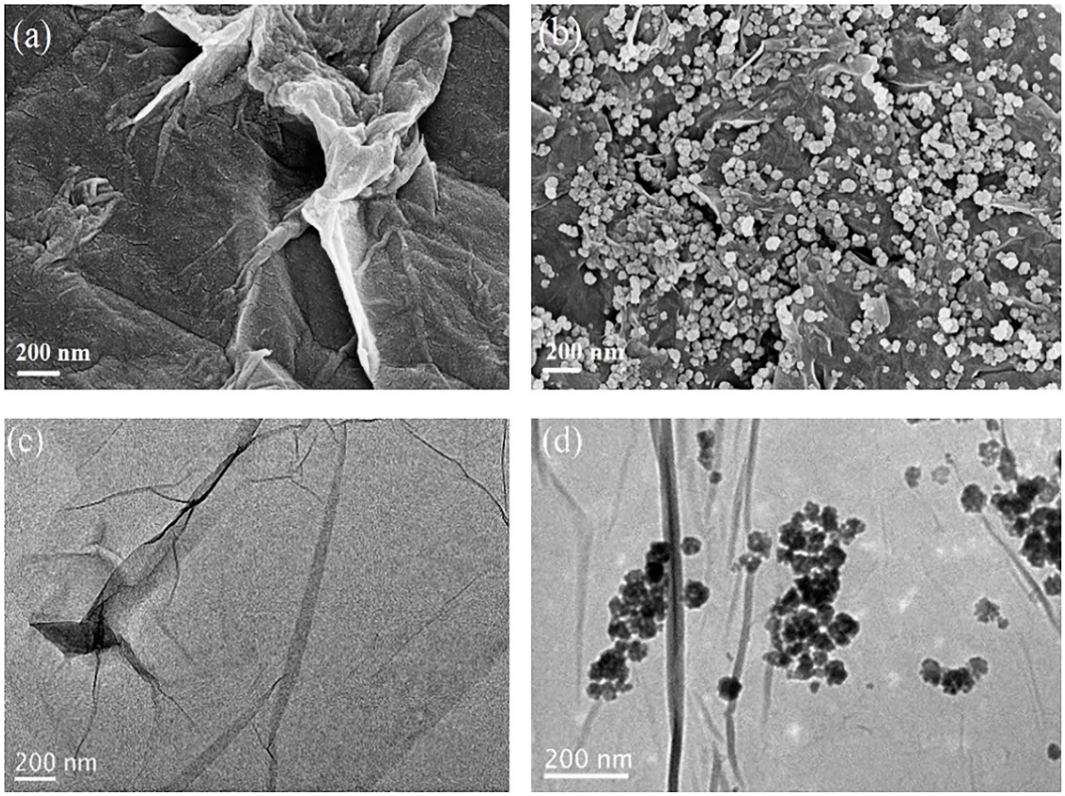

Fig. 2. SEM images of the GO (a) and GO/Fe_3O_4 nanocomposite (b) and TEM images of the GO (c) and GO/Fe_3O_4 nanocomposite (d).

analysis were used. Fig. 2(a) shows a typical morphology of the GO obtained by the improved Hummers methods. It can be seen that GO presents a large sheet of structural thickness, smooth surfaces and wrinkled edges. The GO/Fe_3O_4 nanocomposite exhibited a rough surface (Fig. 2(b)). Meanwhile, distributed dark spots could be seen on the surface of the graphene layer (many Fe_3O_4 nanoparticles were observed on the surface of graphene). As shown in Fig. 3(c), the diameter of Fe_3O_4 NPs in GO/Fe_3O_4 nanocomposite was about 60 nm by measuring at least 100 random nanoparticles in the SEM images using software Image J 1.3s. The Fe_3O_4 NPs were uniformly decorated and firmly anchored on a corrugated graphene layer. The structure of graphene can effectively prevent the Fe_3O_4 NPs from agglomerating and uniformly distributing on the graphene oxide, increasing the active site on the surface of the material.

Similarly, Figs. 2(c) and (d) show TEM images of GO and GO/Fe_3O_4 nanocomposite. There are many oxygenated functional groups, such as hydroxyl, epoxy and carboxyl on the surface of GO sheet [23], so the hydroxylated iron complexes are able to homogeneously anchor onto the surfaces of GO sheets. As can be seen in Fig. 2(d), Fe_3O_4 NPs are grown on GO sheets to form surface-bound nanocomposite, showing a tight bond between the components. GO/Fe_3O_4 nanocomposite retains well-shaped 2D nanostructure of GO sheets, and Fe_3O_4 NPs with uniform diameter are ultradispersed onto GO sheets, with no obvious large or aggregated Fe_3O_4 NPs observed. After dissolving 0.03 g of GO/Fe_3O_4 nanocomposite in 4 mL of HCl, the solution will be cooled to room temperature. Transfer the cooled liquid to a 100 mL volumetric flask and dilute to volume by distilled water. Constant volume solution was sent to ICP-OES for measurement Fe^{3+} concentration. The mass ratio of Fe_3O_4 was calculated to be 58.5%

The XRD patterns of the as-prepared samples were analyzed by X-ray diffractometer as depicted in Fig. 3(a). GO shows a broad peak of the plane approximately at 10.5° with the literature reported [24]. The XRD patterns of Fe_3O_4 NPs and GO/Fe_3O_4 nanocomposite are presented in the figure for comparison. It can be seen from Fig. 3(a) that the GO/Fe_3O_4 peaks of composite material are 18.2°, 30.0°, 35.3°, 42.9°, 53.4°, with the main characteristic peaks of GO/Fe_3O_4 nanocomposite appearing at 56.9° and 62.5°. The characteristic peak position and characteristic peak were consistent with those reported in the literature [22], indicating that the GO/Fe_3O_4 nanocomposite has been successfully synthesized. In addition, the peak of GO/Fe_3O_4 nanocomposite appeared at 24° because of the recovery of part of the graphite crystal structure in the composite after heat treatment [22].

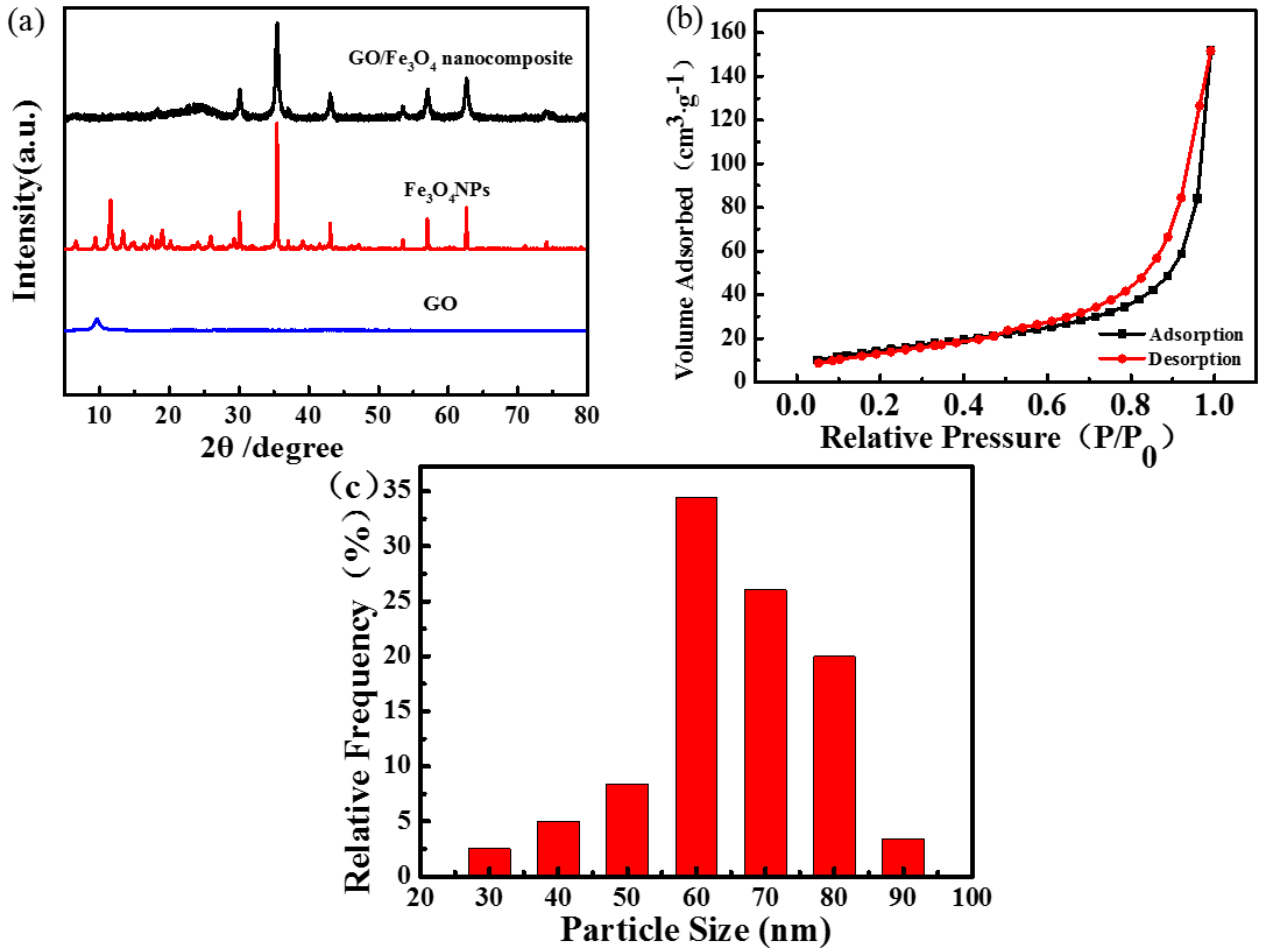

Fig. 3. (a) X-ray diffraction patterns of GO, Fe_3O_4 NPs and GO/Fe_3O_4 nanocomposite; (b) N_2 adsorption/desorption isotherms of GO/Fe_3O_4 nanocomposite and (c) the diameter distribution histograms of Fe_3O_4 NPs.

The adsorbent was further characterized by N_2 adsorption/desorption isotherm. Fig. 3(b) illustrates that the isotherms exhibit type IV shape with H_2 hysteresis loop in the range of 0.50–0.98 relative pressure, indicating the existence of mesoporous structures in the GO/Fe_3O_4 nanocomposite. The BET surface area of the GO/Fe_3O_4 nanocomposite is 54.67 m^2 g^{-1}. Besides, the pore size distribution of the adsorbent was calculated using the Barrett–Joyner–Halenda (BJH) method. The average pore size of GO/Fe_3O_4 nanocomposite adsorption is 16.61 nm and the average pore size of desorption is 14.74 nm. GO/Fe_3O_4 nanocomposite has more pore size than Fe_3O_4 NPs, this change can be attributed to the role of GO in the pore structure of the custom GO/Fe_3O_4 nanocomposite. The BET surface area of GO/Fe_3O_4 nanocomposite is 54.67 m^2 g^{-1}.

Direct evidence for the formation of GO/Fe_3O_4 nanocomposite was provided using a VSM at room temperature with an applied magnetic field of 300 kOe. Fig. 4(a) is the magnetization hysteresis loops of GO/Fe_3O_4 nanocomposite. The saturation magnetization of GO/Fe_3O_4 nanocomposite was 49.46 emu g^{-1}, which is much higher than that of the bare GO/Fe_3O_4 nanocomposite particles reported in previous literature [25]. SEM observation suggested that the magnetic Fe_3O_4 NPs were intimately attached to the surface of graphene oxide which acts as a magnetically inactive layer at the surface of magnetic surface in the composite system, thus affecting the uniformity or magnitude of magnetization. In Fig. 4(a), the value of remanence magnetization and coercivity of the GO/Fe_3O_4 nanocomposite is very low, indicating that GO/Fe_3O_4 nanocomposite is superparamagnetic at room temperature. The superparamagnetic performances suggest that GO/Fe_3O_4 nanocomposite can be easily separated from water by an applied magnetic field as demonstrated in Fig. 4(b). Meanwhile, after removing the magnetic field, GO/Fe_3O_4 nanocomposite can be well dispersed into reaction solution.

3.2. Removal of MG influencing factors by GO/Fe_3O_4 nanocomposite

A series of batch experiments were carried out individually to determine the MG adsorption capacity of the GO/Fe_3O_4 nanocomposite.

Fig. 5 shows the effect of the pH on the adsorption capacity of MG on the GO/Fe_3O_4 nanocomposite. The adsorption capacity of MG on the adsorbent at different pH was 60 mg L^{-1}, the adsorption time was 10 h and the adsorption temperature was 333 K. When the pH is greater than 9, in strong alkali conditions, the solution of OH^- ions will be associated with the MG chemical reaction and cause the solution to fade. The adsorption capacity and removal rate of MB gradually increases with increasing solution pH from 4.0 to 9.0. The reason for this is that pH of the solution can affect the surface charge of the adsorbent due to the presence of a large number of negatively charged oxygen-containing groups in the GO [26,27]. When pH is 4–5, H^+ can compete with the reactive molecules on the adsorbent. The point leads to a decrease in the amount of adsorption. As the pH increases, the electrostatic attraction between the adsorbent and the cationic dye MG increases, resulting in an increase in dye adsorption capacity. The results show that GO/Fe_3O_4 nanocomposite can adsorb MG when pH is 9.

As shown in Figs. 6(a) and (b), the adsorption capacity of the composite increases with increasing initial dye concentration, the absorbance gradually decreases with an

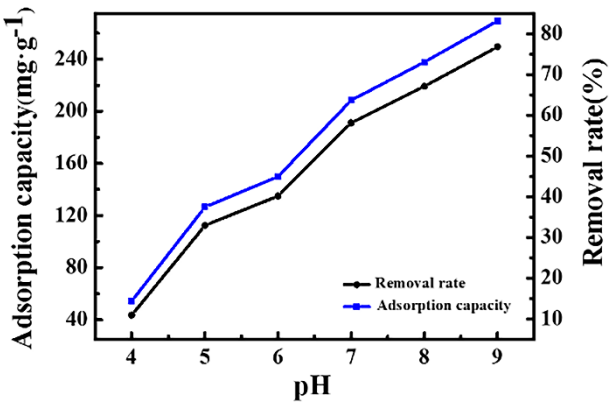

Fig. 5. Effect of solution pH on the adsorption on the GO/Fe_3O_4 nanocomposite (c_0: 60 mg L^{-1}; T: 333 K; t: 10 h; m: 10 mg; V: 50 mL).

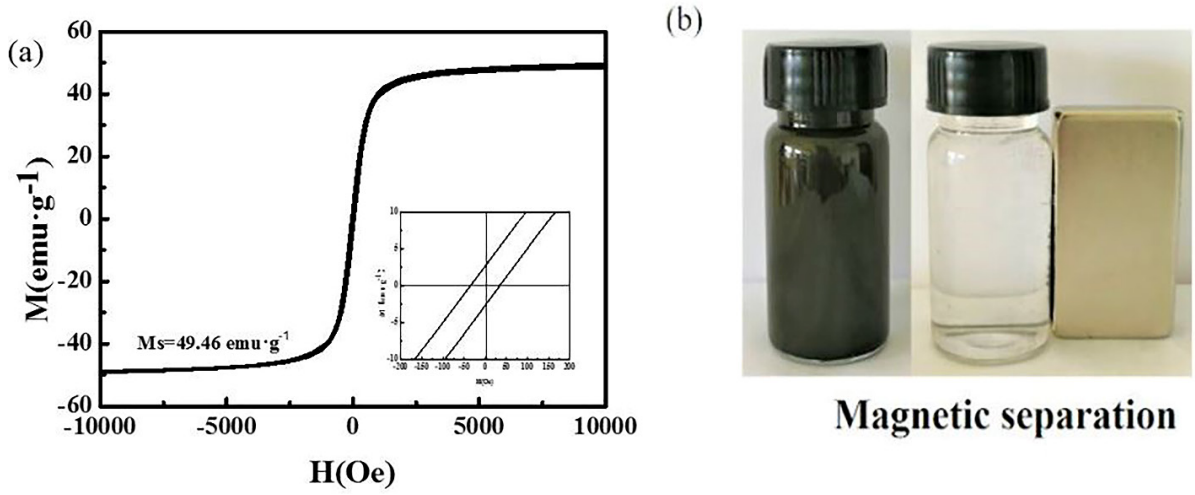

Fig. 4. (a) Hysteresis loops of the GO/Fe_3O_4 nanocomposite and the bottom inset shows close view of the hysteresis loops and (b) the magnetic separation of the GO/Fe_3O_4 nanocomposite under an external magnetic field.

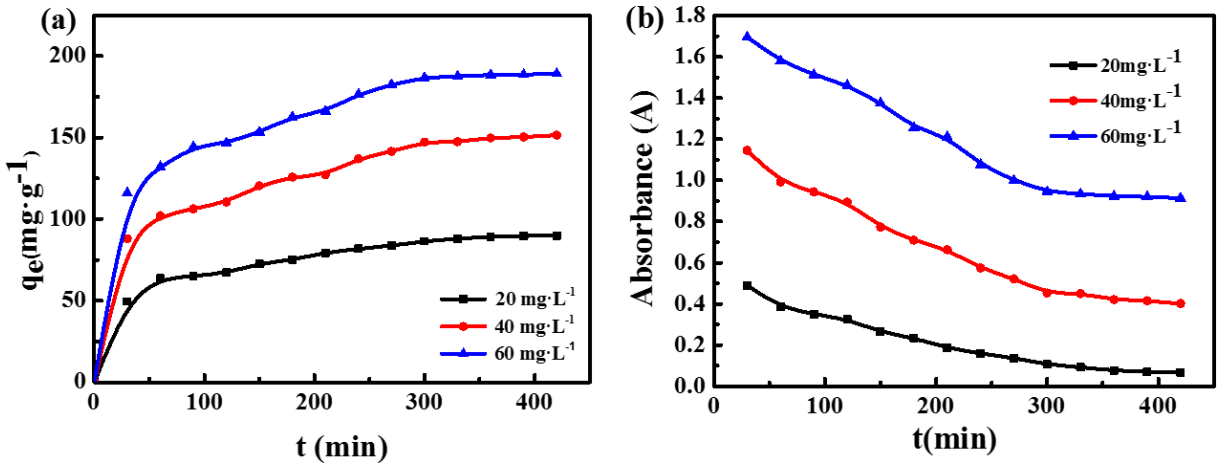

Fig. 6. (a) Time profile of MG adsorption on the GO/Fe_3O_4 nanocomposite with different initial MG and (b) time evolution of the UV–Vis spectra collected each 30 min during MG adsorption on the GO/Fe_3O_4 nanocomposite (*T*: 333 K; *m*: 10 mg; *V*: 50 mL).

increase of time. At higher initial concentrations, more MG molecules can be obtained on the surface of the composite material, resulting in more active sites on the MG molecules and adsorbents. The adsorption capacity of the dye increases as the initial dye concentration increases because more MG molecules are available at higher initial dye concentrations; these concentrations provide higher driving force to overcome the mass transfer resistance of the dye between the aqueous phases and the solid phases, resulting in more collisions between MG molecules and active sites on the adsorbent [28,29]. The amount of adsorbent adsorbed rapidly increased in the first 30 min because of: (1) the electrostatic attraction between the negatively charged oxygen-containing groups and the cationic dye MG on the surface of the adsorbent; (2) MG molecules and GO aromatic π–π bond between the role [30]. Therefore, considering relatively high adsorption capacity, rapid adsorption rate and convenient magnetic reparability, the GO/Fe_3O_4 nanocomposite could be used as a promising alternative adsorbent for dye removal from water.

In addition, the amount of adsorbent affected the adsorption performance (Fig. 7). The dosage of adsorbent increased from 0.2 to 1.0 g L^{-1}, the removal rate of MG increased from 56.4% to 98.2%, and the adsorption capacity of adsorbent on MG decreased from 181.7 to 60.9 mg g^{-1}. This is because the concentration of the adsorbent is too high, resulting in the overlap of the active sites, causing a decrease in the amount of adsorbent. When the amount of adsorbent exceeds 0.6 g L^{-1}, the increase in adsorbent's removal rate of MG is slow. When the amount of adsorbent is 0.8 g L^{-1}, the initial concentration of MG is 60 mg L^{-1}. The concentration of supernatant after adsorption is 1.73 mg L^{-1}. Considering factors such as the removal rate of MG, the economic cost and the adsorption capacity, the amount of adsorbent at 0.8 g L^{-1} is best.

3.3. Adsorption kinetics

To better understand the adsorption mechanism and kinetics, the pseudo-first-order, pseudo-second-order and intra-particle diffusion kinetic models were used to investigate the kinetics of MG adsorption on the GO/Fe_3O_4 nanocomposite. The model was as follows (Eq. (2)–(4)) [31–33]:

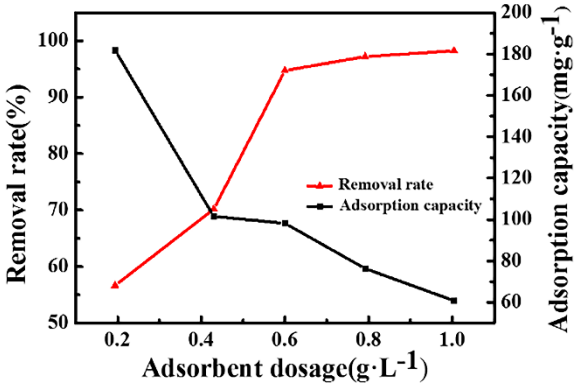

Fig. 7. Effect of adsorbent dose on adsorption of MG by GO/Fe_3O_4 nanocomposite (*T*: 333 K, *t*: 10 h; *m*: 10 mg; *V*: 50 mL).

$$\ln(q_e - q_t) = \ln q_e - kt \tag{2}$$

$$\frac{t}{q_t} = \frac{1}{k_2 q_2^2} + \frac{t}{q_2} \tag{3}$$

$$q_t = \beta \ln(\alpha\beta) + \beta \ln t \tag{4}$$

where t is the adsorption time (min), q_t is the amount of adsorption at time t (mg g^{-1}). q_e and q_2 are the equilibrium adsorption capacities (mg g^{-1}) for the first-order kinetic model and the quasi-second-order kinetic model. k_1 is the primary reaction rate constant (min^{-1}), k_2 is the quasi-secondary reaction rate constant, where α and β are the Elovich constants and represent the initial adsorption rate (g mg^{-1} min^{-1}) and the desorption constant (mg g^{-1} min^{-1}), respectively. The Elovich constants can be obtained from the graphs of q_t vs. ln$t$.

Table 1 and Figs. 8(a)–(c) show the results of quasi-first-order, quasi-second-order kinetic model and Elovich kinetic model for the adsorption of MG by GO/Fe_3O_4 nanocomposite, the quasi-second-order kinetic linear correlation coefficient, the theoretical equilibrium adsorption capacity and the

Table 1
GO/Fe_3O_4 nanocomposite adsorption of MG kinetic parameters

Concentration	$q_{e\text{-exp}}$	Pseudo-first-order kinetics			Pseudo-second-order kinetics			Elovich		
(mg·L^{-1})	(mg·g^{-1})	$k_1 \times 10^2$ (min^{-1})	$q_{e\text{-cal}}$ (mg·g^{-1})	R^2	$k_2 \times 10^{-4}$ g·(mg·min)$^{-1}$	$q_{e\text{-cal}}$ (mg·g^{-1})	R^2	α	β	R^2
20	90	1.272	98.46	0.882	1.833	101.32	0.998	0.0165	18.855	0.990
40	151	1.313	138.91	0.919	1.138	169.21	0.998	0.0135	29.828	0.986
60	189	1.379	188.07	0.907	0.966	212.31	0.999	0.010	38.623	0.981

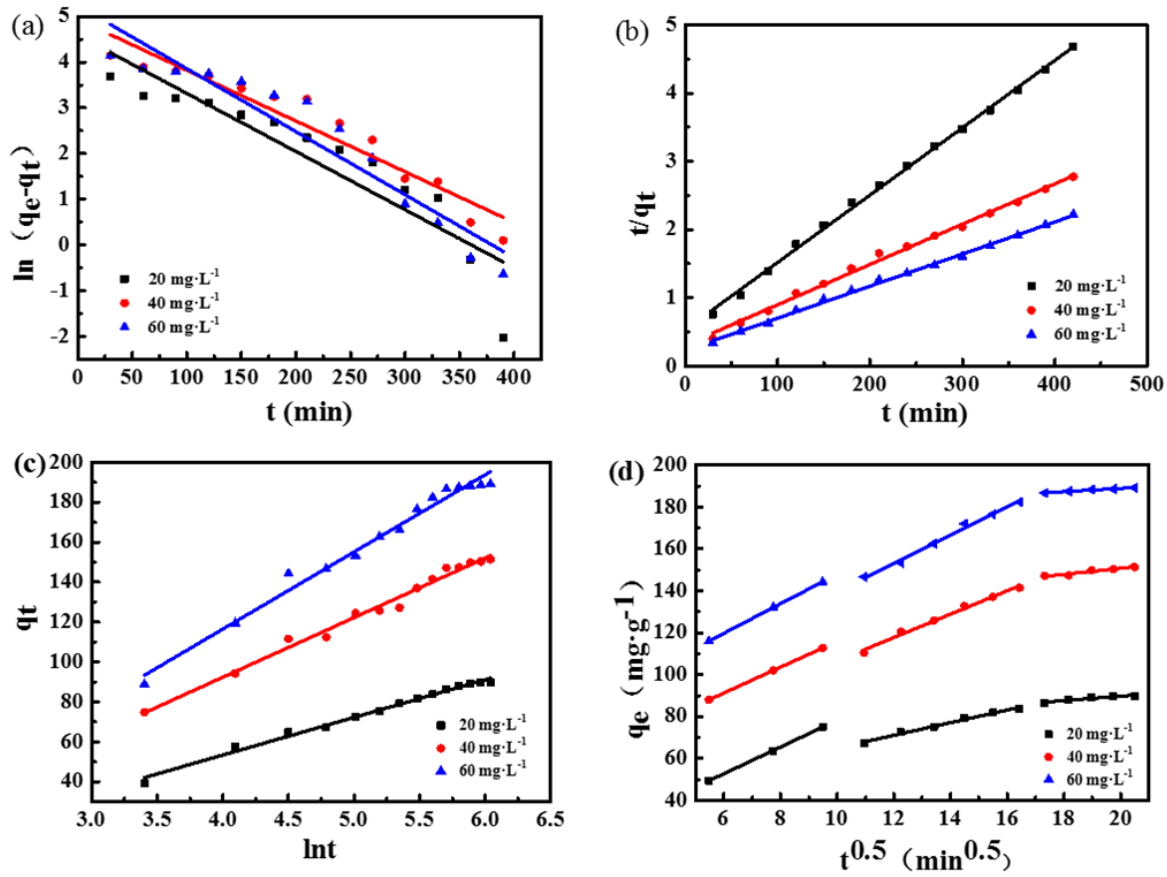

Fig. 8. Pseudo-first-order kinetic model (a), pseudo-second-order kinetic model (b), Elovich kinetic model (c) and intra-particle diffusion kinetic model (d) for the adsorption of MG onto GO/Fe_3O_4 nanocomposite with different initial concentrations.

experimental results. It can be seen that the pseudo-second-order kinetics model is more suitable for the interpretation of the dye adsorption mechanism because the relationship between experimental data and kinetics is determined by applying the correlation coefficient (R^2), it can be seen that the R^2 value of the pseudo-second-order dynamical model is higher than the R^2 value of the pseudo-first-order dynamical model. In addition, the calculated q_e value is also consistent with the experimental data. Therefore, the adsorption of MG by the magnetic material is in accordance with the pseudo-second-order kinetic equation.

The adsorption kinetics of MG on the solid particles is controlled by the following three steps: (1) boundary diffusion, (2) MG adsorption on the surface of solid particles and (3) internal diffusion [34]. The internal diffusion model is as follows:

$$q_e = k_p t^{0.5} + B \tag{5}$$

where k_p (mg g^{-1} min$^{0.5}$) is the particle diffusion rate constant. B is the adsorption constant. If we plot $q_e - t^{0.5}$, we can get a straight line, indicating that the whole adsorption process is controlled by the diffusion within the particle, and if it is straight and through the origin, it is the only constant speed step. If the multi-linearity is plotted with $q_e - t^{0.5}$, it indicates that the adsorption process is a complex process controlled by multiple velocity steps. As shown in Fig. 8(c), the kinetic data are fitted with three-stage linearity by intra-particle diffusion model, indicating that the adsorption process which is complex is divided into three stages: the adsorption of MG at the first stage adsorbent increases with $t^{0.5}$ and significantly increased, which corresponds to the diffusion of

the boundary layer of MG. In the second stage, the adsorption of MG on the adsorbent increases with an increase of $t^{0.5}$, but the slope of the second line is smaller and the adsorption capacity increases more slowly than in the first stage, because the second stage is controlled by particle diffusion. The third stage of adsorption tends to saturate, which means that the adsorption reaches equilibrium stage. Therefore, the process of adsorption MG was not only controlled by the intra-particle diffusion but also by the membrane diffusion.

3.4. Isothermal adsorption line

The adsorption behavior of GO/Fe_3O_4 nanocomposite on MG was simulated by Langmuir, Freundlich and Temkin adsorption models. The model is as follows (Eqs. (6)–(8)) [35–37]:

$$\frac{c_e}{q_e} = \frac{1}{Q_m K_L} + \frac{c_e}{Q_m} \tag{6}$$

$$\ln q_e = \ln K_F + \frac{\ln c_e}{n} \tag{7}$$

$$q_e = B \ln K_T + B \ln c_e \tag{8}$$

where c_e (mg L^{-1}) is the equilibrium concentration of MG. q_e (mg·g^{-1}) for the amount of adsorbent adsorbed MG. Q_m (mg·g^{-1}) is maximum adsorption capacity, K_L (L·mg^{-1}) is the balance constant. K_F and $1/n$ represent the Freundlich constant of adsorption capacity and adsorption intensity, respectively. B and K_T (L g^{-1}) are the constants.

Isotherm studies can describe how the adsorbates interact with adsorbents, affording the most important parameter for designing a desired adsorption system. The adsorption isotherms of MG on the GO/Fe_3O_4 nanocomposite at different initial concentrations are given in Figs. 9(a)–(c). As shown in Table 2, which summarizes the Langmuir, Freundlich and Temkin constants and the calculated coefficients, the Freundlich equation correlation coefficient of GO/Fe_3O_4 nanocomposite adsorbed MG indicates that the adsorption of MG onto GO/Fe_3O_4 nanocomposite is in agreement with

Table 2
Langmuir, Freundlich and Temkin parameters for adsorption of MG by GO/Fe_3O_4 nanocomposite at different temperature

Isothermal	Parameter	313 K	323 K	333 K
Langmuir equation	Q_m (mg·g^{-1})	220	317	336
	K_L (L·mg^{-1})	0.21	0.29	0.37
	R^2	0.960	0.972	0.994
Freundlich equation	K_F (mg·g^{-1})	70.940	88.146	92.516
	$1/n$	0.338	0.321	0.420
	R^2	0.870	0.757	0.686
Temkin equation	B (L·g^{-1})	45.074	50.130	76.865
	K_T (L·g^{-1})	3.344	4.675	2.615
	R^2	0.922	0.870	0.826

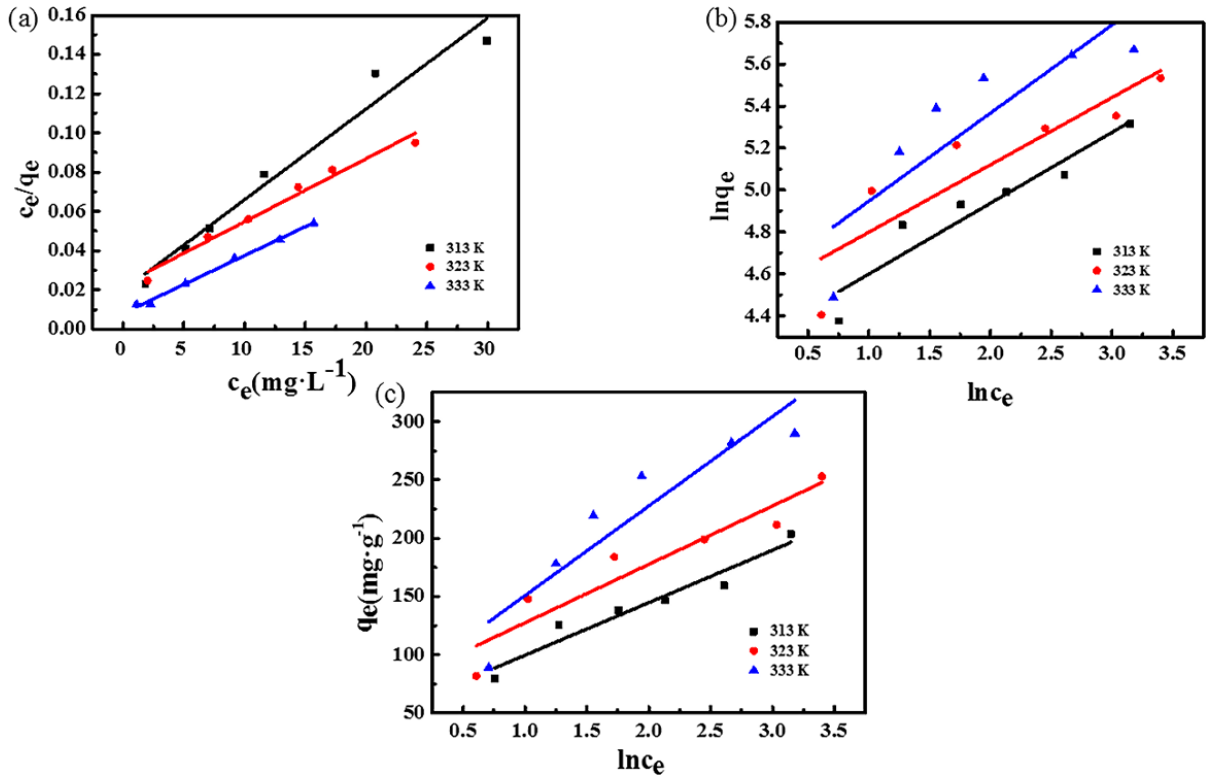

Fig. 9. Langmuir (a), Freundlich (b) and Temkin (c) isotherm model for MG adsorption onto GO/Fe_3O_4 nanocomposite at different temperatures.

Langmuir. The adsorption of MG onto GO/Fe_3O_4 nanocomposite is also in agreement with Langmuir. The addition of the Freundlich equation at different temperatures of 313, 323, 333 K is greater than 1, indicating that GO/Fe_3O_4 nanocomposite is easy to adsorb MG preferential adsorption.

In order to determine whether an adsorption system is "favorable" or "unfavorable" between the adsorbent and the adsorbate, R_L, the separation factor or equilibrium parameter, is also calculated using Eq. (9) [38]:

$$R_L = \frac{1}{1+bc_0} \tag{9}$$

where b (L mg^{-1}) is the Langmuir constant and c_0 (mg L^{-1}) is the initial dye concentration. The value of R_L indicates the shape of the isotherm to be either unfavorable ($R_L > 1$), linear ($R_L = 1$), favorable ($0 < R_L < 1$) or irreversible ($R_L = 0$) [39]. The R_L values between 0 and 1 indicate favorable adsorption. For MG adsorption on the GO/Fe_3O_4 nanocomposite, the R_L values obtained are far less than 1, thereby confirming that the adsorption is a favorable process.

3.5. Adsorption thermodynamics

To study the inherent energy changes within the adsorption process, the thermodynamic parameters of the adsorption were investigated. The change in the Gibbs free energy (ΔG), enthalpy (ΔH) and entropy (ΔS) was calculated from the following Eqs. (10) and (11) [40]:

$$\Delta G = -RT\ln K_D \tag{10}$$

$$\ln K_D = \frac{\Delta S}{R} - \frac{\Delta H}{RT} \tag{11}$$

where R is the gas constant (8.314 J mol^{-1} K^{-1}), K_D is the distribution coefficient ($K_D = q_e/c_e$), ΔH and ΔS can be calculated from the slope of the curve and intercept of the calculated temperature of the adsorption of MG thermodynamic parameters shown in Fig. 10 and Table 3.

The negative ΔG indicates that the adsorption of MG on GO/Fe_3O_4 nanocomposite was carried out spontaneously. The adsorption value was 256.37 and 75.16 kJ mol^{-1}. This is greater than zero and indicates that the degree of confusion in the adsorption process is increased because the adsorption of a large number of water molecules at the solid/liquid interface is greater than zero. This indicates that the GO/Fe_3O_4 nanocomposite adsorbed MG is an endothermic process, which is conducive to the promotion of the adsorption temperature. More than 40 kJ mol^{-1} indicates that the adsorption process is chemisorption, less than 40 kJ mol^{-1}, indicates that the adsorption process is physical adsorption, 75.16 kJ mol^{-1} is greater than 40 kJ mol^{-1}, indicating that the adsorption process is chemical adsorption [40]. A positive value of ΔS means that randomness at the solid–solution interface increases during the adsorption. At all three temperature $|\Delta S| > |\Delta H|$, demonstrating that the adsorption is dominated by entropy effect rather than enthalpy change.

Table 3
Thermodynamic parameters of MG in GO/Fe_3O_4 nanocomposite adsorbed water

Temperature (K)	K_D (L·mg^{-1})	ΔG (kJ·mol^{-1})	ΔS (J mol^{-1} K^{-1})	ΔH (kJ·mol^{-1})
313	7.79	–5.342		
323	13.82	–7.052	256.37	75.16
333	42.17	–10.359		

3.6. Regeneration

The stability and regeneration ability of the adsorbent is crucial for its practical application. The cycles of adsorption–desorption experiments were also carried out as shown in Fig. 11(a). After once, twice, three times, four times, after regeneration, the saturated adsorption capacity was 83.6%, 80.2%, 77.7% and 73.1%, respectively. It can be found that the adsorption capacity did not decrease apparently. After four cycles, the adsorption rate reduced by only 10%. The XRD patterns and SEM images of regenerated GO/Fe_3O_4 nanocomposite are shown in Figs. 11(b)–(d). Compared with the XRD of fresh GO/Fe_3O_4 nanocomposite, the XRD pattern of the regenerated GO/Fe_3O_4 nanocomposite did not change significantly. Meanwhile, the SEM morphology after regeneration also showed that the crystal shape did not change significantly. In addition, the use of magnetic separation GO/Fe_3O_4 nanocomposite recovery, when the initial input amount of 10 mg, the recovery rate can reach 90.27% ± 4.46%, compared with other materials recycle, such as an activated electric arc furnace slag (A-EAFS) [41], Fe_3O_4/activated montmorillonite (Fe_3O_4/Mt) [42], the usage of a composite of zinc sulfide nanoparticles with activated carbon (ZnS–NPs–AC) [43], indicating that the GO/Fe_3O_4 nanocomposite has relatively good stability and reusability.

3.7. Comparison with other adsorbents

It can be seen from Table 4 that the adsorption capacity of GO/Fe_3O_4 nanocomposite to MG is higher than that of other materials. The reason for this phenomenon is due to the presence of electrostatic attraction between the negatively charged oxygen-containing groups on the GO/Fe_3O_4 nanocomposite surface and the cationic MG and the effect of the

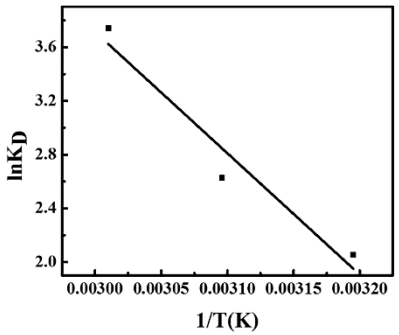

Fig. 10. Plot of lnK_D vs. 1/T for MG dye adsorption by GO/Fe_3O_4 nanocomposite (c_0: 60 mg L^{-1}; t: 10 h; m: 10 mg; V: 50 mL).

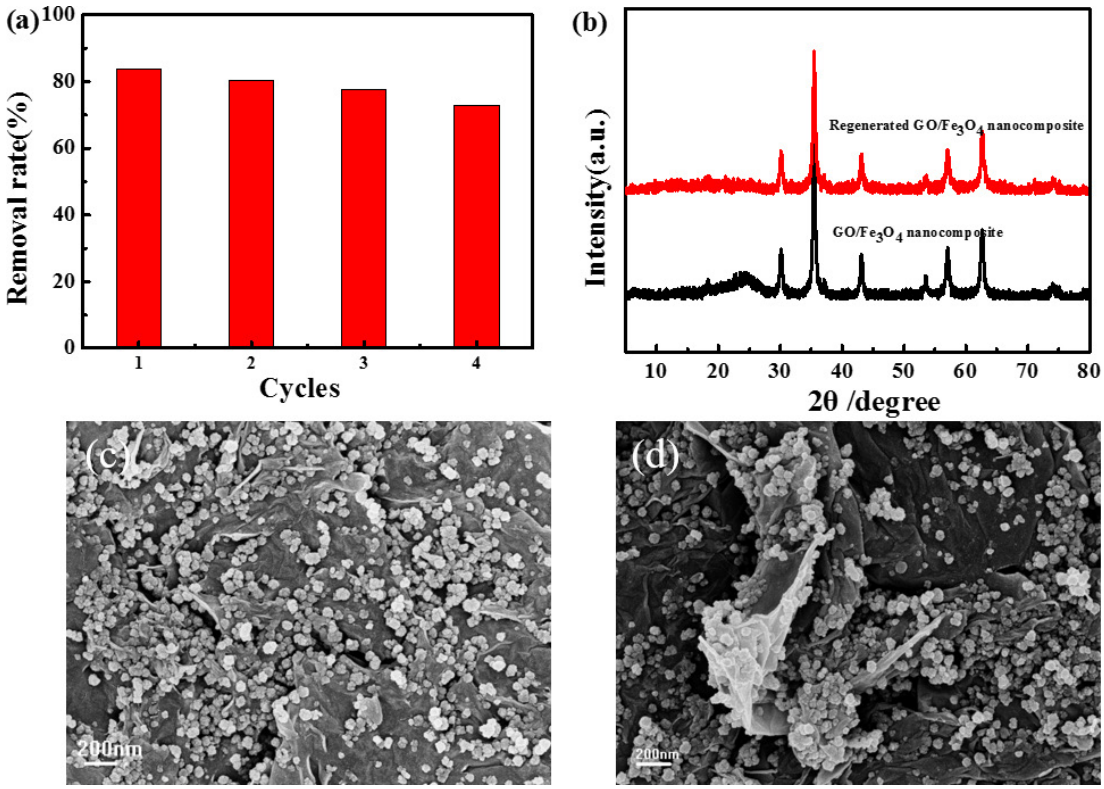

Fig. 11. (a) Recycling of GO/Fe_3O_4 nanocomposite on MG adsorption; (b) XRD patterns of GO/Fe_3O_4 nanocomposite and forth-regenerated GO/Fe_3O_4 nanocomposite. SEM images of (c) GO/Fe_3O_4 nanocomposite and (d) forth-regenerated GO/Fe_3O_4 nanocomposite.

Table 4
Comparison of q_e for different adsorbents

Serial number	Adsorbents	q_e ($mg \cdot g^{-1}$)	References
1	GO/Fe_3O_4 nanocomposite	220	This study
2	Glutamate-functionalized sawdust	197	[44]
3	Graphene oxide-agarose hydrogel	186	[45]
4	Sepiolite/cellulose hybrid bead (SCB)	314	[46]
5	Cattail biomass–based activated carbon	210	[47]
6	Wood apple shell	35	[48]
7	Activated carbon derived from durian seed	32	[49]
8	Aluminum(III)-based MOF (MIL-53(Al)-NH_2)	141	[50]
9	Cellulose modified with maleic (M) anhydride	370	[51]
10	Cellulose modified with phthalic (P) anhydride	111	[51]
11	Carboxylate-functionalized adsorbent	150	[52]
12	Cellulose-based adsorbent	132	[53]
13	Treated ginger waste	188	[54]

π–π bond between the MG molecule and the GO aromatic compound. Compared with the material filtration and separation in Table 4, such as Cattail biomass–based activated carbon [47], CMA [51] and CMGT [53], the material can be quickly separated by external magnetic field to avoid secondary pollution and the preparation process is simple and economical. This study provides an easy way to prepare highly efficient magnetic nanomaterials adsorbents to remove MG from water. These advantages are not available in other materials displayed in Table 4.

4. Conclusions

In summary, a GO/Fe_3O_4 nanocomposite was prepared as an efficient adsorbent for MG uptake by a solvothermal method loading of Fe_3O_4 NPs on the surface of graphene oxide. The adsorbent was separated from the dye solution quickly by an additional magnetic field to avoid secondary pollution. The results indicated that the process is in accordance with the quasi-second-order kinetics equation and the Freundlich adsorption model. Besides, the adsorption thermodynamic parameters indicate that this process is spontaneous and endothermic. The magnetic composite has strong adsorption capacity for MG in water with a saturated adsorption capacity of 220 mg g^{-1}. In addition, π–π and electrostatic interactions are assumed to be the main causes of high adsorbent adsorption. The regeneration of the adsorbent showed that GO/Fe_3O_4 nanocomposite has remarkable potential for dye removal even after four adsorption–desorption cycles. This study indicates that the as-prepared GO/Fe_3O_4

nanocomposite could be utilized as a magnetically separable and efficient adsorbent for the removal of MG from aqueous solution.

Acknowledgment

The present research is supported by the Natural Science Foundation of China (No. 41371446 and No. 41271498).

References

[1] J.V. Valh, A.M.L. Marechal, S. Vajnhandl, T. Jerič, E. Šimon, Water in the textile industry, Treatise Water Sci., 4 (2011) 685–706.
[2] Y.J. Tan, L.J. Sun, B.T. Li, X.H. Zhao, T. Yu, N. Ikuno, K. Ishii, H.Y. Hu, Fouling characteristics and fouling control of reverse osmosis membranes for desalination of dyeing wastewater with high chemical oxygen demand, Desalination, 419 (2017) 1–7.
[3] X. Zhu, X. Jiang, S. Cheng, K. Wang, S. Mao, L.J. Fan, Preparation of high strength ultrafine polyvinyl chloride fibrous membrane and its adsorption of cationic dye, J. Polym. Res., 17 (2010) 769–777.
[4] I. Savva, O. Marinica, C.A. Papatryfonos, L. Vekas, T. Krasia-Christoforou, Evaluation of electrospun polymer–Fe_3O_4 nanocomposite mats in malachite green adsorption, RSC Adv., 5 (2015) 16484–16496.
[5] B. Samiey, A.R. Toosi, Adsorption of malachite green on silica gel: effects of NaCl, pH and 2-propanol, J. Hazard. Mater., 184 (2010) 739–745.
[6] L. Sun, S. Hu, H. Sun, H. Guo, H. Zhu, M. Liu, H. Sun, Malachite green adsorption onto Fe_3O_4@SiO_2-NH_2: isotherms, kinetic and process optimization, RSC Adv., 5 (2015) 11837–11844.
[7] S. Babak, T.A. Raoof, Kinetics of malachite green fading in alcohol–water binary mixtures, Int. J. Chem. Kinet., 42 (2010) 508–518.
[8] M. Tichonovas, E. Krugly, V. Racys, R. Hippler, V. Kauneliene, I. Stasiulaitiene, D. Martuzevicius, Degradation of various textile dyes as wastewater pollutants under dielectric barrier discharge plasma treatment, Chem. Eng., 229 (2013) 9–19.
[9] A. Witek-Krowiak, Biosorption of malachite green from aqueous solutions by pine sawdust: equilibrium, kinetics and the effect of process parameters, Desal. Wat. Treat., 51 (2013) 3284–3294.
[10] F. Aydin, E. Yilmaz, M. Soylak, A simple and novel deep eutectic solvent based ultrasound-assisted emulsification liquid phase microextraction method for malachite green in farmed and ornamental aquarium fish water samples, Microchem. J., 132 (2017) 280–285.
[11] X. Wei, X. Kong, C. Sun, J. Chen, Characterization and application of a thin-film composite nanofiltration hollow fiber membrane for dye desalination and concentration, Chem. Eng., 223 (2013) 172–182.
[12] M.H. Do, N.H. Phan, T.D. Nguyen, T.T. Pham, V.K. Nguyen, T.T. Vu, T.K. Nguyen, Activated carbon/Fe_3O_4 nanoparticle composite: fabrication, methyl orange removal and regeneration by hydrogen peroxide, Chemosphere, 85 (2011) 1269–1276.
[13] F. Basiri, M. Feiz, A. Moheb, Recycling of direct dyes wastewater by nylon-6 nanofibrous membrane, Curr. Nanosci., 7 (2011) 633–639.
[14] X. Fang, S. Xiao, M. Shen, R. Guo, S. Wang, X. Shi, Fabrication and characterization of water-stable electrospun polyethyleneimine/polyvinyl alcohol nanofibers with super dye sorption capability, New J. Chem., 35 (2011) 360–368.
[15] K.N. Gupta, N.J. Rao, G.K. Agarwal, Gaseous phase adsorption of volatile organic compounds on granular activated carbon, Chem. Eng. Commun., 202 (2015) 384–401.
[16] N. Listed, The rise and rise of graphene, Nat. Nanotechnol., 5 (2010) 755–760.
[17] S. Kashyap, S. Mishra, S.K. Behera, Aqueous colloidal stability of graphene oxide and chemically converted graphene, J. Nanopart., 2014 (2014) 1240–1245.
[18] M. Zhou, F. Pu, Z. Wang, T. Cai, H. Chen, H. Zhang, S. Guan, Facile synthesis of novel Si nanoparticles-graphene composites as high-performance anode materials for Li-ion batteries, Phys. Chem. Chem. Phys., 15 (2013) 11394–11401.
[19] Y.K. Lv, J. Zhang, M.Z. Li, S.D. Zhou, X.H. Ren, J. Wang, Fast clean-up and selective enrichment of florfenicol in milk by restricted access media molecularly imprinted magnetic microspheres based on surface-initiated photoiniferter-mediated polymerization, Anal. Methods, 8 (2016) 3982–3989.
[20] A. Altinisik, Y. Seki, S. Ertas, E. Akar, E. Bozacı, Y. Seki, Evaluating of *Agave americana* fibers for biosorption of dye from aqueous solution, Fibers Polym., 16 (2015) 370–377.
[21] A.S.M.I. Uddin, G.S. Chung, Synthesis of highly dispersed ZnO nanoparticles on graphene surface and their acetylene sensing properties, Sens. Actuators B, 205 (2014) 338–344.
[22] L. Ai, C. Zhang, Z. Chen, Removal of methylene blue from aqueous solution by a solvothermal-synthesized graphene/magnetite composite, J. Hazard. Mater., 192 (2011) 1515–1524.
[23] N.A. Zubir, C. Yacou, J. Motuzas, X. Zhang, J.C.D.D. Costa, Structural and functional investigation of graphene oxide–Fe_3O_4 nanocomposites for the heterogeneous Fenton-like reaction, Sci. Rep., 4 (2014) 4594–4602.
[24] T.K. Sahu, S. Arora, A. Banik, P.K. Iyer, M. Qureshi, Efficient and rapid removal of environmental malignant Arsenic (III) and industrial dyes using re-usable, recoverable ternary Iron Oxide-ORMOSIL-Graphene Oxide composite, ACS Sustainable Chem. Eng., 5 (2017) 5912–5921.
[25] J. Wang, W. Xu, L. Chen, X. Huang, J. Liu, Preparation and evaluation of magnetic nanoparticles impregnated chitosan beads for arsenic removal from water, Chem. Eng. J., 251 (2014) 25–34.
[26] H. Kim, S.W. Kim, Y.U. Park, H. Gwon, D.H. Seo, Y. Kim, K. Kang, SnO_2/graphene composite with high lithium storage capability for lithium rechargeable batteries, Nano Res., 3 (2010) 813–821.
[27] T.H. Han, W.J. Lee, D.H. Lee, J.E. Kim, E.Y. Choi, S.O. Kim, Peptide/graphene hybrid assembly into core/shell nanowires, Sci. Technol. Adv. Mater., 22 (2010) 2060–2064.
[28] M. Ghaedi, A. Hassanzadeh, S.N. Kokhdan, Multiwalled carbon nanotubes as adsorbents for the kinetic and equilibrium study of the removal of alizarin red s and morin, J. Chem. Eng. Data, 56 (2011) 2511–2520.
[29] L. Ai, J. Jiang, Fast removal of organic dyes from aqueous solutions by AC/ferrospinel composite, Desalination, 262 (2010) 134–140.
[30] W. Fan, W. Gao, C. Zhang, W.T. Weng, J. Pan, T. Liu, Hybridization of graphene sheets and carbon-coated Fe_3O_4 nanoparticles as a synergistic adsorbent of organic dyes, J. Mater. Chem., 22 (2012) 25108–25115.
[31] A. Bhatnagar, W. Hogland, M. Marques, M. Sillanpää, An overview of the modification methods of activated carbon for its water treatment applications, Chem. Eng. J., 219 (2013) 499–511.
[32] Y.S. Ho, G. Mckay, Pseudo-second order model for sorption processes, Process Biochem., 34 (1999) 451–465.
[33] J. Abdi, M. Vossoughi, N.M. Mahmoodi, I. Alemzadeh, Synthesis of metal-organic framework hybrid nanocomposites based on GO and CNT with high adsorption capacity for dye removal, Chem. Eng. J., 326 (2017) 1145–1158.
[34] Y. Ma, S.G. Wang, M. Fan, W.X. Gong, B.Y. Gao, Characteristics and defluoridation performance of granular activated carbons coated with manganese oxides, J. Hazard. Mater., 168 (2009) 1140–1146.
[35] Y. Zhan, J. Lin, J. Li, Preparation and characterization of surfactant-modified hydroxyapatite/zeolite composite and its adsorption behavior toward humic acid and copper(II), Environ. Sci. Pollut. Res., 20 (2013) 2512–2526.
[36] Y. Song, K. Qu, C. Zhao, J. Ren, X. Qu, Graphene oxide: intrinsic peroxidase catalytic activity and its application to glucose detection, Adv. Mater., 22 (2010) 2206–2210.
[37] I. Langmuir, The adsorption of gases onplane surfaces of glass, J. Chem. Phys., 40 (2015) 1361–1403.
[38] T.W. Weber, R.K. Chakravorti, Pore and solid diffusion models for fixed-bed adsorbers, AlChE J., 20 (2010) 228–238.

[39] G. Mckay, Adsorption of dyestuffs from aqueous solutions with activated carbon II: column studies and simplified design models, J. Chem. Technol. Biotechnol., 32 (1982) 773–780.
[40] Y. Hashimoto, K. Tokura, H. Kishi, W.M.J. Strachan, Prediction of seawater solubility of aromatic compounds, Chemosphere, 13 (1984) 881–888.
[41] N. Nasuha, S. Ismail, B.H. Hameed, Activated electric arc furnace slag as an effective and reusable Fenton-like catalyst for the photodegradation of methylene blue and acid blue 29, J. Environ. Manage., 196 (2017) 323–329.
[42] J. Chang, J. Ma, Q. Ma, D. Zhang, N. Qiao, M. Hu, H. Ma, Adsorption of methylene blue onto Fe_3O_4/activated montmorillonite nanocomposite, Appl. Clay Sci., 119 (2015) 132–140.
[43] A. Asfaram, M. Ghaedi, M.H.A. Azqhandi, A. Goudarzi, M. Dastkhoon, Statistical experimental design, least square-support vector machine (LS-SVM) and artificial neural network (ANN) methods for modeling of facilitated adsorption of methylene blue dye, RSC Adv., 6 (2016) 40502–40516.
[44] B. Tao, A.J. Fletcher, Metaldehyde removal from aqueous solution by adsorption and ion exchange mechanisms onto activated carbon and polymeric sorbents, J. Hazard. Mater., 244–245 (2013) 240–250.
[45] R. Gong, M. Feng, J. Zhao, W. Cai, L. Liu, Functionalization of sawdust with monosodium glutamate for enhancing its malachite green removal capacity, Bioresour. Technol., 100 (2009) 975–978.
[46] X. Jiang, S. Wang, L. Ge, F. Lin, Q. Lu, T. Wang, B. Huang, B. Lu, Development of organic–inorganic hybrid beads from sepiolite and cellulose for effective adsorption of malachite green, RSC Adv., 7 (2017) 38965–38972.
[47] M. Yu, Y. Han, J. Li, L. Wang, CO_2-activated porous carbon derived from cattail biomass for removal of malachite green dye and application as supercapacitors, Chem. Eng. J., (2017) 493–502.
[48] A.S. Sartape, A.M. Mandhare, V.V. Jadhav, P.D. Raut, M.A. Anuse, S.S. Kolekar, Removal of malachite green dye from aqueous solution with adsorption technique using *Limonia acidissima* shell as low cost adsorbent, Arabian J. Chem., 10 (2013) 3229–3238.
[49] M.A. Ahmad, N. Ahmad, O.S. Bello, Adsorptive removal of malachite green dye using durian seed-based activated carbon, Water Air Soil Pollut., 225 (2014) 2057–2074.
[50] C. Li, Z. Xiong, J. Zhang, C. Wu, The Strengthening Role of the Amino Group in Metal–Organic Framework MIL-53 (Al) for Methylene Blue and Malachite Green Dye Adsorption, J. Chem. Eng. Data, 60 (2015) 3414–3422.
[51] Y. Zhou, Y. Min, H. Qiao, Q. Huang, E. Wang, T. Ma, Improved removal of malachite green from aqueous solution using chemically modified cellulose by anhydride, Int. J. Biol., 74 (2015) 271–277.
[52] H. Qiao, Y. Zhou, F. Yu, E. Wang, Y. Min, Q. Huang, L. Pang, T. Ma, Effective removal of cationic dyes using carboxylate-functionalized cellulose nanocrystals, Chemosphere, 141 (2015) 297–303.
[53] Y. Zhou, X. Wang, M. Zhang, Q. Jin, B. Gao, T. Ma, Removal of Pb(II) and malachite green from aqueous solution by modified cellulose, CELLULOSE, 21 (2014) 2797–2809.
[54] R. Ahmad, R. Kumar, Adsorption studies of hazardous malachite green onto treated ginger waste, J. Environ. Manage., 91 (2010) 1032–1038.